MODELING OF VISCOUS FLOWS IN TWO-DIMENSIONAL TURBOMACHINERY CASCADE VIA VISCOUS-INVISCID INTERACTION METHOD

M. Z. Yusoff, I. Hussein, T. Yusaf and Z. Ahmad

Department of Mechanical Engineering, College of Engineering, Universiti Tenaga Nasional , 43009 Kajang, Selangor.

ABSTRACT

A two-dimensional time-accurate time-marching viscous flow solver employing the viscous-inviscid interaction method suitable for turbomachinery applications is described. The inviscid main flow solver uses the second-order accurate cell-vertex finite-volume spatial discretisation and fourth-order accurate Runge-Kutta temporal integration. The viscous effect due to boundary layer development on the blade surfaces and wakes are modelled using an independent one-dimensional boundary layer subroutine capable of modelling laminar, transition and fully turbulent flows. The solver has been applied to subsonic, transonic and supersonic flow in a cascade of nozzle blades. The results are compared with the experimental data and they showed very good agreement.

Keywords : *Boundary Layer, CFD, Time-Marching, Turbine, Turbomachinery, Viscous,*

1.0. INTRODUCTION

Flow in real turbomachines is very complex being three-dimensional, unsteady, viscous and turbulent. However, in many cases, considerable physical insights into the phenomena involved can be gained by simplifying the flow. Wu [1] showed that, the general three-dimensional flow within a turbomachine can be reasonably described by a combination of two-dimensional solutions in two different planes. As shown in Figure 1, the first family is referred to as *S1* or blade-to-blade plane and the second one as *S2* or meridional plane. The solutions on *S2* plane provide information about the mean flow through the turbine, while *S1* solutions give information about flow behaviour round individual blade sections. Instead of solving the full three-dimensional equations, considerable saving can be gained by solving the two-dimensional equations and iterate between the two planes. [2] has developed a robust, two-dimensional on *S1* plane time-accurate inviscid Euler solver suitable for turbomachinery applications under transonic flow conditions. The program was applied to transonic flow in a cascade of nozzle blade and shows remarkable agreement with experimental data in terms of blade surface static pressure distributions and overall flow features within the cascade. However the program could not predict the expansion efficiency of the blade because the extra losses due to the boundary layer effects and wakes were not modelled. The present paper describes the extension of the program to include the viscous effect due to boundary layer and wakes. The method used is the viscous-inviscid interaction method via an independent one-dimensional boundary layer subroutine. In this method, the main flow is regarded to be inviscid and governed by the Euler equation. The viscous effect, as suggested by Prandtl, is assumed to be concentrated in the thin boundary layer region next to the blade surface. This main Euler solver and the boundary layer subroutine are coupled and applied alternately until convergence by using the viscous-inviscid interaction method. Similar methods have been used in [3,4].

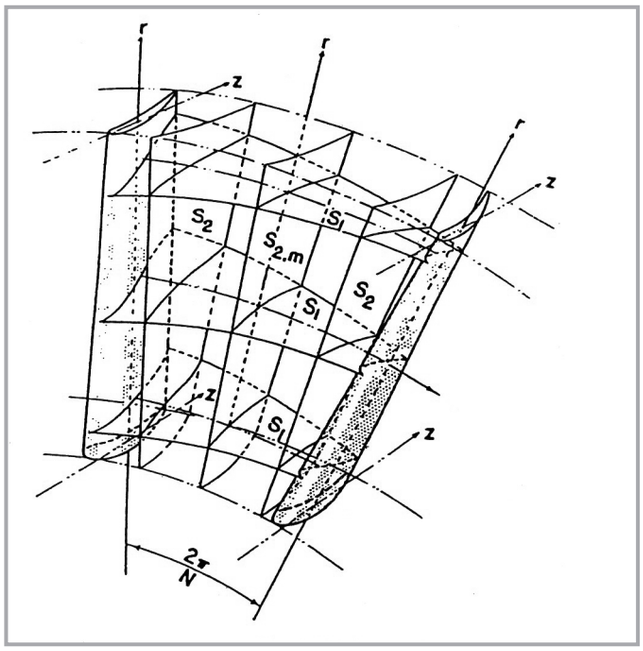

***Figure 1: S1 and S2 stream surfaces* [1])**

In this paper the numerical formulations which are used to solve the governing equations is discussed. This is followed by the discussion on the Integral viscous-inviscid integral boundary layer method. Finally the program is applied to transonic flows in cascade of turbine blades and the results are compared with the experimental measurements.

2.0. NUMERICAL FORMULATIONS

The governing equations employed are the time dependent Euler equations. The main flow governing equations cast in the finite volume formulation in x-y cartesian coordinates system

is : -

$$\Omega \frac{\partial \underline{w}}{\partial t} = -\oint_S (\underline{F}dy - \underline{G}dx) \tag{1}$$

where

$$\underline{w} = \begin{vmatrix} \rho \\ \rho V_x \\ \rho V_y \\ \rho E_0 \end{vmatrix} \qquad \underline{F} = \begin{vmatrix} \rho V_x \\ \rho V_x{}^2 + P \\ \rho V_x V_y \\ \rho V_x H_0 \end{vmatrix} \qquad \underline{G} = \begin{vmatrix} \rho V_y \\ \rho V_y V_x \\ \rho V_y{}^2 + P \\ \rho V_y H_0 \end{vmatrix} \tag{2}$$

Ω is the volume of the small element with perimeter S as shown in Figure 2. The small element shown is one of the finite volumes which are formed by the intersection of quasi-streamlines and quasi-orthogonal lines. The flow variables are stored at the cell vertices. In this paper, only a brief description of the numerical formulations will be given. Detail descriptions can be obtained in [2]. The above equations are solved simultaneously for each finite cell volume using a time marching method.

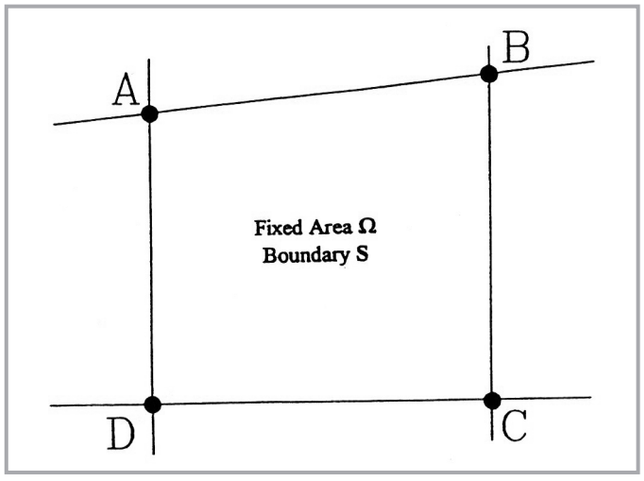

Figure 2: An element of a H-mesh

The spatial integration is done using central discretisation which is of second order accuracy. A blend of second and fourth order artificial dissipations with pressure switch are added to the residuals prior to the time integration to remove wiggles from the solution. The temporal integration is done using the fourth order accurate, 4 stage Runge Kutta time stepping method. To speed up the convergence, 3 types of convergence acceleration schemes are employed namely, local time-stepping, enthalpy damping and implicit residual averaging.

At inlet boundary, the total pressure, total temperature and flow angle are fixed while the static pressure is extrapolated from the interior. At exit, if the exit flow is subsonic, only the static pressure is fixed, while total pressure, total temperature and flow angle are extrapolated from the interior. If the exit flow is supersonic, all four variables are extrapolated from the interior. The periodicity condition on the bounding streamlines, upstream and downstream of the blade row, is easily satisfied by treating the calculating points on each of the bounding streamline as if they were interior ones. At the solid boundary, normal fluxes are set to zero.

3.0. INTEGRAL BOUNDARY LAYER METHOD

The boundary layer subroutine covers the laminar boundary layers, natural transition and transition through bubble separation, turbulent boundary layers and wakes. The routine was originally developed in [5] and modified to suit the current inviscid flow solver.

Laminar Boundary Layer

The method of [6] has been adopted due to its simplicity and adequate accuracy. This method consists of the numerical integration of the momentum integral equation, using auxiliary relationships for skin friction and shape factor as functions of pressure gradient parameter, Λ. Thwaites showed that the momentum thickness, θ , is given by : -

$$\Delta\theta^2 = \frac{0.45\nu}{\overline{V}_e^6} \int_0^x V_e^5 \, dx \tag{3}$$

where, the bar over V_e denotes the average value over an increment Δx.

In order to calculate the skin friction coefficient and the displacement thickness, the modified expressions for $L(\Lambda)$ and $H(\Lambda)$ as given in [7] are used. δ^* and C_f can be evaluated as : -

$$\delta^* = H\theta \tag{4}$$

$$C_f = \frac{\tau_{wall}}{\frac{1}{2}\rho_e V_e^2} = \frac{2\nu}{V_e^2}\left(\frac{\partial V}{\partial y}\right)_{y=0} = \frac{2\nu}{V_e\theta} L(\Lambda) \tag{5}$$

Laminar-Turbulent Transition

Boundary layer transition from laminar to turbulent flow can occur either by natural transition or laminar separation bubble ending in re-attachment as a turbulent boundary layer.

In natural transition, there is a gradual increase in the proportion of the flow which is turbulent at any instant (intermitency) from zero to one. Natural transition is assumed to occur when the momentum thickness Reynolds number reaches a critical value, which is a function of the pressure gradient parameter and the turbulence level.

In a laminar separation bubble, the laminar boundary layer separates and forms a laminar free shear layer which eventually undergoes transition to turbulence. The turbulent free shear layer gains sufficiently high energy fluid from the free-stream by diffusion to reattach as a turbulent boundary layer. Bubble transition occurs if the pressure gradient parameter, Λ, falls below -0.09. The bubble length and the condition on reattachment are determined by two empirical correlations in [8]. The flow was assumed to undergo transition to turbulence at the start of bubble separation. It is also assumed that boundary layer transition occurs instantaneously upon interaction with a shockwave.

Turbulent Boundary Layer

The lag-entrainment method originated in [9] is used in the treatment of turbulent boundary layers. This method employs three differential equations; the momentum integral equation, the entrainment equation and an equation describing the streamwise rate of change of entrainment coefficient. The first two equations are those used in Head's original treatment, the

last one is an equation for shear stress developed by [10]. The method also allows a first-order approximation for compressibility. The three equations are as follows : -

$$\frac{d\theta}{dx} = \frac{C_f}{2} - \left(H + 2 - Ma_e^2\right)\frac{\theta}{V_e}\frac{dV_e}{dx} \quad (6)$$

$$\theta\frac{d\overline{H}}{dx} = \frac{d\overline{H}}{dH_1}\left\{C_E - H_1\left(\frac{C_f}{2} - \left(H+1\right)\frac{\theta}{V_e}\frac{dV_e}{dx}\right)\right\} \quad (7)$$

$$\theta\frac{dC_E}{dx} = F\left\{\frac{2.8}{H+H_1}\left[\left(C_\tau\right)_{EQ0}^{\frac{1}{2}} - \lambda_b C_\tau^{\frac{1}{2}}\right] + \left(\frac{\theta}{V_e}\frac{dV_e}{dx}\right)_{EQ}\right.$$

$$\left. - \frac{\theta}{V_e}\frac{dV_e}{dx}\left[1 + 0.075Ma_e^2\,\frac{1+0.2Ma_e^2}{1+0.1Ma_e^2}\right]\right\} \quad (8)$$

where, Ma_e is free-stream Mach number, C_τ is the shear stress coefficient, λ_b is the overall scaling factor and suffices *EQ* and 0 indicate the values in equilibrium flow and zero pressure gradient respectively.

The auxiliary relations for other boundary layer parameters; C_f, H, H_1, dH / dH_1, C_τ and F in the above equations are that given by [4]. Equilibrium flows are defined as those in which the shape of the velocity and shear stress profiles in the boundary layer do not vary with distance, x. Therefore, throughout the flow, dH/dx and $d(C_\tau)_{max}/dx$ are both zero. The auxiliary equations for the equilibrium quantities are taken from expressions recommended in [11].

The boundary layer growth is calculated by the simultaneous forward integration of the three differential equations using Runge-Kutta technique for the three independent variables, momentum thickness, θ, transformed shape factor, H and the entrainment coefficient, C_E. The distribution of displacement thickness, δ^* and other boundary layer parameters are obtained from these.

Treatment of Wake

The basic equations governing the flow in boundary layers are equally applicable to wakes. Thus, the treatment of attached boundary layers described above can be applied to wakes with only minor modifications. The skin friction, *Cf* is set to zero and the overall scaling factor, λb is halved.

4.0. NUMERICAL PROCEDURES

In the viscous-inviscid interaction procedure, the inviscid free-stream flow for a given blade geometry is first determined and then the boundary layer displacement thickness corresponding to the blade inviscid velocity distribution is evaluated. The displacement thickness on both suction and pressure surfaces are then added in order to modify the blade geometry. The process is then repeated until the solutions converge. In the numerical solution, the boundary layer calculation is called at 400th time step and subsequently at an interval of 200 time steps until the solutions converge.

The boundary layer is initially laminar around the leading edge, but the pressure distribution obtained in this region is affected by numerical errors. For this reason, the start of the boundary layer treatment is delayed for a distance equivalent to about 2-3 % of the blade chord. At the starting point, the values of θ and C_f are assumed to be zero and 0.025 respectively. This simplification has little effect on the accuracy because the displacement and momentum thickness are very small in this region.

5.0. BLADE PROFILE LOSS

The profile loss of a turbine blade is defined as the loss due to boundary layer growth on the blade surface and the subsequent dissipation in the blade wake. The boundary layer loss is calculated by : -

$$Bl_{loss} = 1 - \left(1 - \frac{\theta}{Pitch - \delta^*}\right)^2 \text{ x } 100\ \% \quad (9)$$

where θ and δ^* represent the summation of their values on the suction and pressure sides at the trailing edge plane. The mixing loss is given by : -

$$Mixing_{loss} = \frac{K.E. - \frac{1}{2}\left(\overline{V}_{x\,mix}^2 + \overline{V}_{y\,mix}^2\right)}{K.E.} \text{ x } 100\ \% \quad (10)$$

6.0. RESULTS

The flow solver and the boundary layer routine were applied to flows over cascade of a nozzle blade profile. The blade profile belongs to a stator of a low pressure steam turbine. The general shape of the profile is shown in Figure 3. Experimental measurements have been performed in [12] in the blow-down tunnel. The measurements undertaken include surface pressure measurements, wake traverses and optical observations by Mach-Zhender interferometry and shadow-graph. The calculations were performed for three flow conditions similar to the experiments covering subsonic, sonic

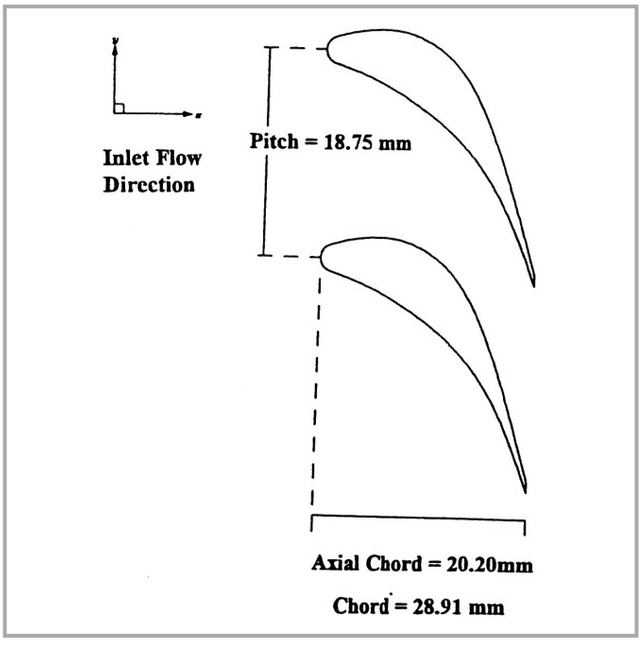

Figure 3: The overall geometry of the nozzle blade cascade

and supersonic flows. The corresponding pressure ratio P_{oinlet}/P_b are 1.49, 1.83 and 2.32 for subsonic, sonic and supsrsoic flows respectively. Figure 4 shows the mesh arrangements used which consists of 33 x 230 grids. There are 52 elements upstream of the blade passage, 130 within the passage and 48 downstream. The details of the mesh at the leading and trailing edges are also shown. The initial mesh orientation downstream of the blade was set parallel to the blade outlet angle, but the final orientation of the downstream periodic boundaries emerged from the solution.

A typical comparison of measured and calculated values of blade surfaces and mid passage static pressure distributions for supersonic flow case at pressure ratio 2.32 is shown in Figure 5. The corresponding contours of constant Mach numbers are shown in Figure 6 together with the Mach-Zhender photograph obtained in the experiment. It can be seen that the agreement between measurements and predictions are very good. At this pressure ratio, it can be seen that there are two shockwaves springed from the trailing edge. One trailing edge shockwave impinged the suction surface at approximately 80 % axial chord and the other one crosses the blade passage. The location of these shockwaves have been predicted very well. Results of the static pressure distributions and mach number contours and comparisons with at other pressure ratios have been described in details in [2] and will not be described here.

The distributions of the displacement, momentum thicknesses, momentum thickness Reynolds number, mean velocity shape factor and skin friction coefficient for both blade pressure and suction surfaces at pressure ratio 2.32 are shown in Figures 7, 8, 9, 10 and 11 respectively. It can be seen that the boundary layer remains laminar on the pressure surface throughout. The boundary layer is initially thinner on the suction surface but the position is reversed at about 80 % axial chord and is mainly due to the effect of external velocity field. With reference to Figure 10, the value of mean velocity shape factor shows that the boundary layer is laminar up to about 80 % axial chord on the suction surface. At that location, the momentum thickness Reynolds number increases sharply. This is caused by the shockwave originating from the pressure side trailing edge, impinging on the suction surface. Bubble separation is noticeable at this point and the skin friction falls to zero. The flow is assumed to undergo transition to turbulence instantaneously. Because of this assumption, there is a small drop in displacement thickness as shown in Figure 7. Immediately downstream of the trailing edge, there is a sudden drop in displacement thickness. This is a consequence of the assumptions made for the turbulent boundary layer parameters at the start of the wake in which the skin friction is set to zero and the overall scaling factor is halved.

The overall accuracy of the boundary layer calculations can be determined by comparing the measured and calculated expansion efficiency. The predicted total loss is the summation of boundary layer, mixing and shock losses. The overall losses

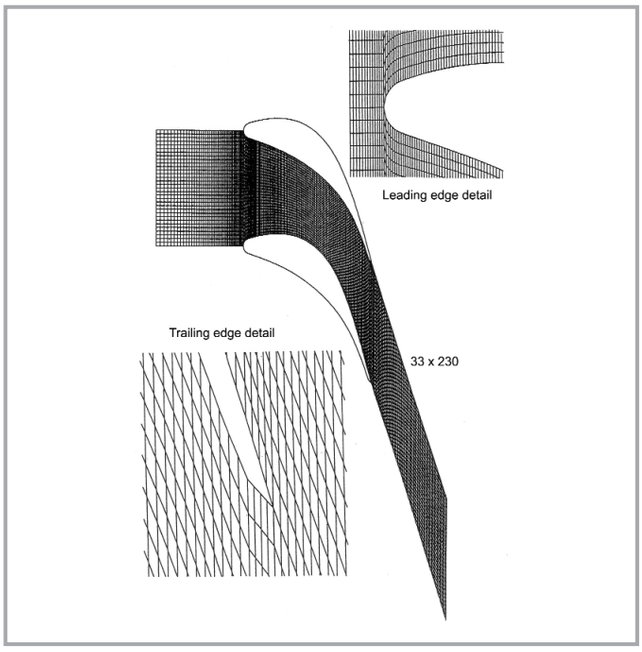

Figure 4: H-mesh used in the calculations for the nozzle blade cascade

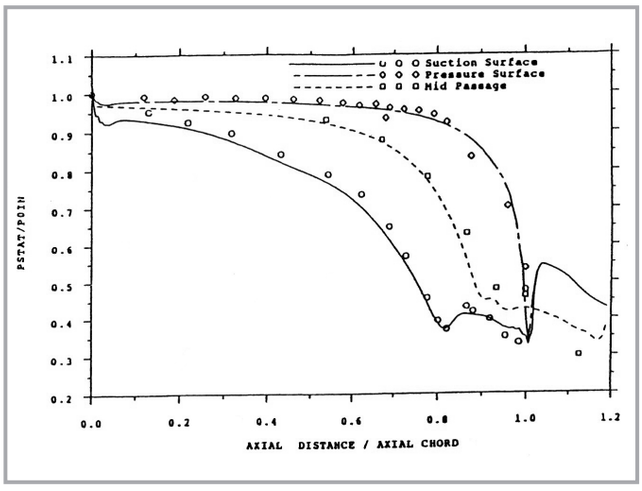

Figure 5: Comparisons of measured and calculated static pressure distributions for the nozzle cascade in supersonic flow condition

for all the three flow conditions are shown in Table 1. The shock loss is estimated by using the oblique shock tables. The experimental measurement of the cascade overall expansion efficiencies which have been carried out in [12] are also given. At pressure ratio of 2.32, the calculated efficiency of 97.02 % which compares well with the measured value of 96.23 %. Similarly for pressure ratios 1.83 and 1.48, the predicted efficiencies are 96.28 and 97.27 respectively which are very close to the experimental measurement in [12] , 96.06 and 97.61

Table 1: Overall losses for all three flow conditions

Flow Condition	Press Ratio	Boundary Layer Loss%	Mixing Loss%	Shock Loss%	Efficiency%	
					Pred	Exp
Supersonic	2.33	1.55	0.96	0.474	97.02	96.23
Sonic	1.83	2.25	1.34	0.131	96.28	96.07
Subsonic	1.48	2.37	0.37	-	97.27	97.61

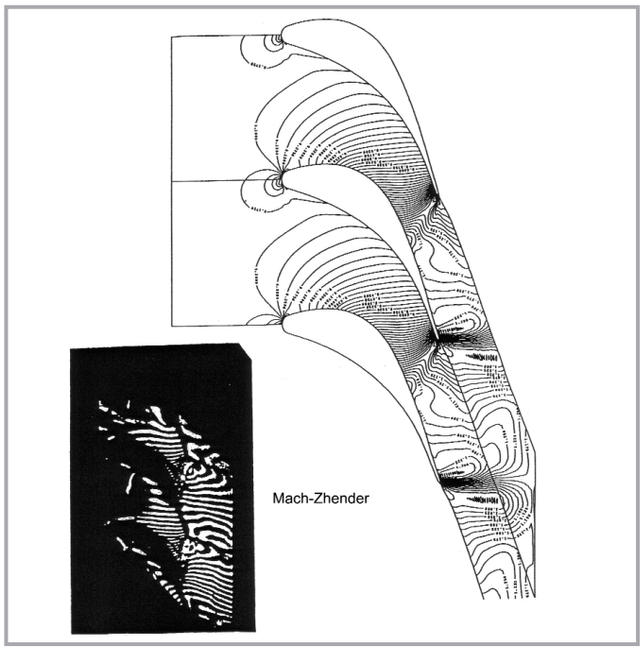

Figure 6: Contour of constant Mach number for the nozzle cascade in supersonic flow condition and observed Mach Zhender photograph

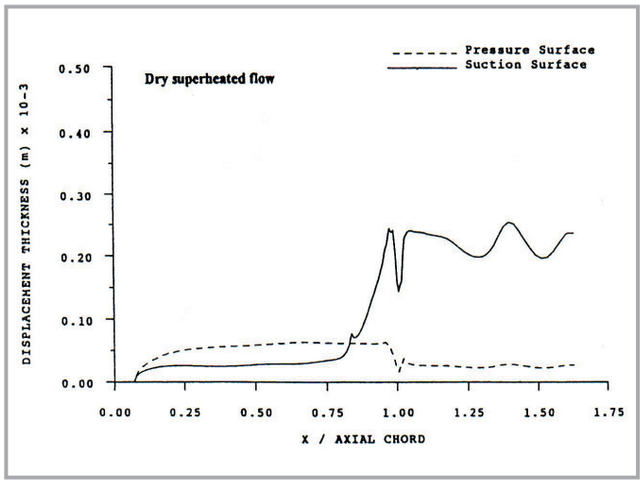

Figure 7: Distribution of displacement thickness on the blade surfaces

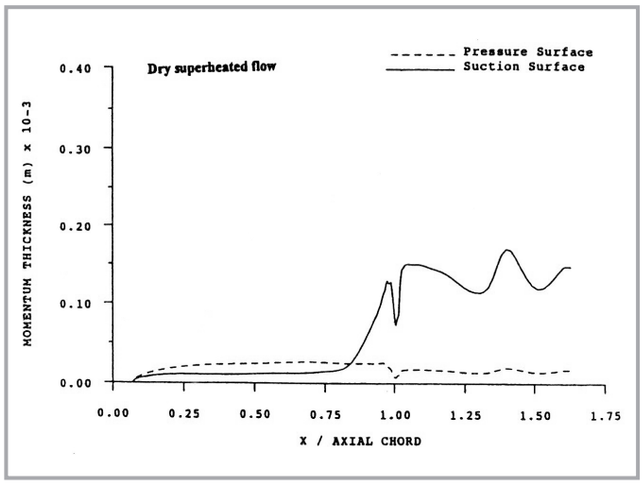

Figure 8: Distribution of momentum thickness on the blade surfaces

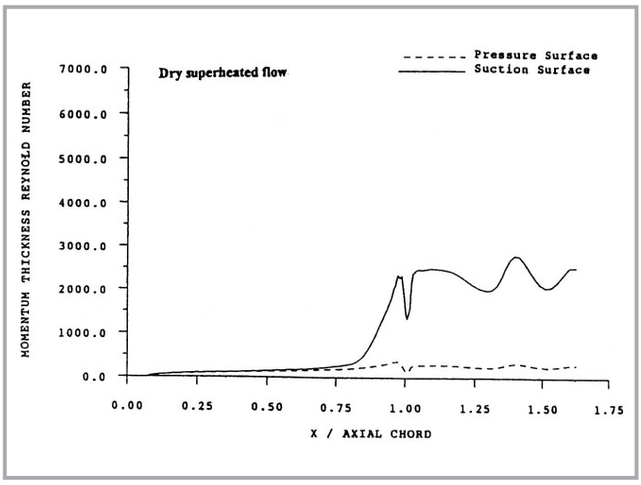

Figure 9: Distribution of momentum thickness Reynolds number on the blade surfaces

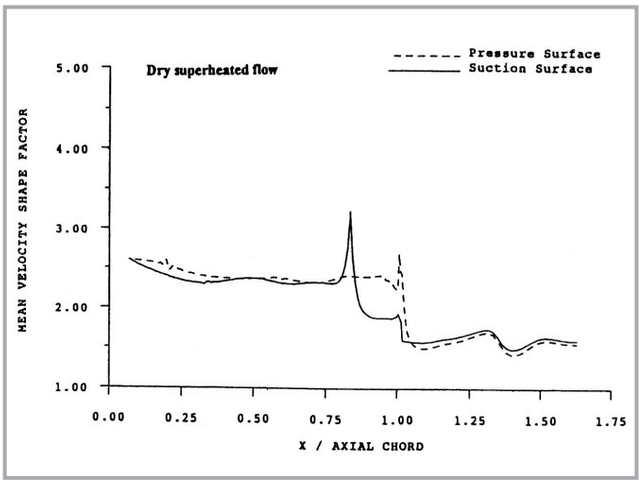

Figure 10: Distribution of mean velocity shape factor on the blade surfaces

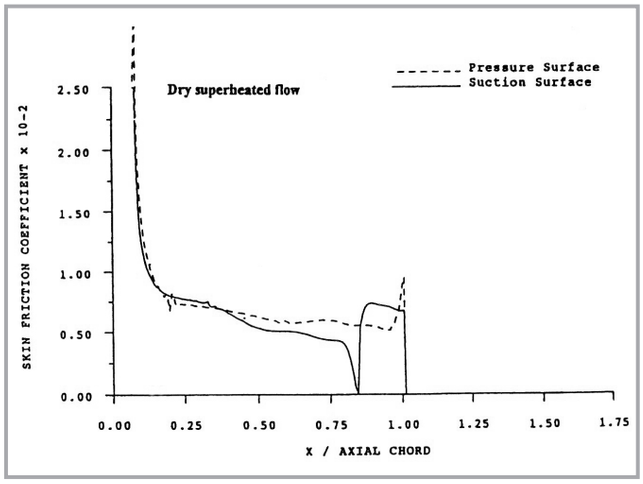

Figure 11: Distribution of skin friction coefficients on the blade surfaces

respectively. It should be noted that no base pressure losses are included in the treatment which explains the slightly higher values of efficiencies at sonic and supersonic flows compared to experimental data. At subsonic flow, the predicted value is slightly lower than the experimental measurement. It can be

concluded that the boundary layer calculation is able to accurately predict the loss accurately.

7.0. CONCLUSIONS AND FUTURE WORKS

The development of a two-dimensional viscous flow solver for turbomachinery applications is described. The solver made use of an independent boundary layer calculations which is integrated with the inviscid Euler solver with the viscous-inviscid interaction method. The comparisons with the experimental data has shown that the boundary layer calculation is able to accurately predict the loss. However, because of the nature of the viscous-inviscid interaction method, it is not possible to predict the direct interaction between the boundary layer and main flow field such as shock boundary layer interaction. In order to predict this, direct inclusion of the viscous term including the turbulence terms into the governing equations are needed. The next step of the work is the inclusion of these terms into the governing equations. ■

NOMENCLATURE

Symbol	Meaning
$Bl_{Total\ loss}$	Total boundary layer loss
Bl_{loss}	Boundary layer loss
C_E	Entrainment coefficient
C_f	Skin friction coefficient
C_{fo}	Skin friction coefficient in equilibrium flow in zero pressure gradient
C_τ	Shear stress coefficient
F_C	Scaling function in skin friction law
$\underline{F_C}$	x component of the inviscid flux vector
F_R	Scaling function in skin friction law
$\underline{F_V}$	x component of the viscous flux vector
H	Mean velocity shape factor
$\overline{H}$	Transformed shape factor
H_1	Mass flow shape factor
$Mixing_{loss}$	Mixing loss
P	Static pressure
P_o	Stagnation pressure
P_b	Downstream static pressure
R_C	Inviscid component of the flux residual
R_x	Reynolds number based on the axial distance
R_θ	Reynolds number based on momentum thickness
r	Droplet radius
r_T	Temperature recovery factor
T	Temperature
t	Time
Δt	Time step for main calculation
V	Overall velocity
V_e	Free stream velocity
V_x	Velocity component in x direction
V_y	Velocity component in y direction
$\underline{w}$	Conserved variable vector
x	Axial distance

GREEK SYMBOLS

Symbol	Meaning
ρ	Density
λ_b	Overall scaling factor on dissipation length
Λ	Thwaites pressure gradient parameter
τ	Shear stress
δ	Overall boundary layer thickness
δ^*	Displacement thickness
δ_3	Energy thickness
θ	Momentum thickness
Ω	Volume of element
Δ	Mass flow thickness

SUBSCRIPT

Symbol	Meaning
e	Values at the edge of the boundary layer
EQ	Denotes equilibrium conditions.
$EQ0$	Denotes equilibrium conditions in absence of secondary influences on turbulent structure
$inlet$	inlet plane values
o	Stagnation condition or values free from secondary effluence
$wall$	Values at the wall
x	Cartesian co-ordinates
y	Cartesian co-ordinates
∞	Edge of boundary layer

REFERENCES

[1] Wu, Chung-Hua, [1952] "A General Theory of Three-Dimensional Flow in Subsonic and Supersonic Turbomachines of Axial Radial and Mixed-Flow Types", NASA TN 2604

[2] Yusoff, M.Z. [1998] "A Two-Dimensional Time-Accurate Euler Solver for Turbomachinery Applications", Journal Institution of Engineers, Malaysia, Vol. 59, No. 3.

[3] Mahpeykar, M.R. [1991] "On the Theoretical Treatment of Two-dimensional Flows of Steam and Comparison with Measurements", Ph.D Thesis, University of Birmingham

[4] Singh, U.K. [1980] "Shock Boundary Layer Interaction in Turbomachine", Von Karman Institute Lecture Series.

[5] Abbas, K., [1987] "An Investigation of Viscous 2-D, 2-Phase Flows in Cascades of Steam Turbine Blading by the Time Marching Method", Ph.D. Thesis, University of Birmingham

[6] Thwaites, B. [1949] "Approximate Calculation of the Laminar Boundary Layer", Aero. Quarterly, Vol. 1, pp. 245-280.

[7] Cebeci, T. [1977] "Calculation of Laminar and Turbulent Boundary Layers for 2-d Time Dependent Flows", N.A.C.A. C.R., No. 2820.

[8] Horton, H.P. [1968] "Laminar Separation Bubbles in Two and Three Dimensional Incompressible Flow", P.h.D. Thesis, Queen Mary College, Dept. of Aero. Eng.

[9] Head, M.R. [1958] "Entrainment in Turbulent Boundary Layer", A.R.C. R. and M. No. 3152, September 1958.

[10] Bradshaw, P., Ferriss, D.H. and Atwell, N.P. [1967] "Calculation of Boundary Layer Development Using the Turbulent Energy Equation", J. Fluid Mech., Vol. 28, Part 3, pp. 593-616

[11] Green, J.E., Weeks, D.J. and Brooman, J.W.F. [1973] "Prediction of Turbulent Boundary Layer and Wakes in Compressible Flow by Lag Entrainment Method" A.R.C., R. and M., No. 3791.

[12] Mamat, Z.A. [1996] "The Performance of a Cascade of Nozzle Turbine Blading in Nucleating Steam", Ph.D. Thesis, Department of Manufacturing and Mechanical Engineering, The University of Birmingham, U.K.

PROFILE

Dr Mohd. Zamri Yusoff
Dr Mohd. Zamri Yusoff is currently a senior lecturer and the deputy dean of the College of Engineering, Universiti Tenaga Nasional (UNITEN). He obtained his PhD (Mechanical Engineering) from the University of Birmingham, UK in 1997. His research interest is in Computational Fluid Dynamics (CFD), numerical modeling, turbomachinery, condensation and energy-related studies.

Prof. Dr. Ibrahim Hussein
Assoc. Prof. Dr. Ibrahim Hussein is currently the Deputy Vice Chancellor (Academics) of the Universiti Tenaga Nasional (UNITEN). He obtained his PhD in Mechanical Engineering from the University of Liverpool, UK in 1992. His research interests are in Energy utilization, steam metering, thermal environment and other energy related studies.

Dr. Talal Yusaf
Dr. Talal Yusaf is currently an Associate Professor in the Department of Mechanical Engineering, College of Engineering, Universiti Tenaga Nasional (UNITEN). He obtained his PhD in Mechanical Engineering from Universiti Kebangsaan Malaysia (UKM) in 2000. His areas of specializations are biotechnology and combustion.

Zulkifli Ahmad
Zulkifli Ahmad is currently a lecturer in the Department of Mechanical Engineering, College of Engineering, Universiti Tenaga Nasional (UNITEN). He obtained his Master of Mechanical Engineering from UNITEN in 2004. His research interests are in CFD and other energy related studies.

ANNOUNCEMENT

Dear IEM Members/Readers,

REFEREES FOR VETTING OF IEM PUBLICATIONS

The Standing Committee on Publications is revising the list of referees to assist in the vetting of articles received from members and non-members. The referees should preferably be at least Corporate Members of the Institution or graduates with higher degrees.

The aim of appointing the referee is to ensure and maintain a standard in the IEM Publications namely the bulletin and the Journal.

Members who interested to be placed in the **database of referees** are to return the registration form to the IEM Secretariat, providing details of their degrees and particular expertise and experience in the engineering fields.

We need your services to look into the vetting of articles received for Publications and due acknow-ledgement would be announced yearly in the Bulletin. Referees must be committed to return the papers within a month from date of appointment.

For your information, vetting of each completed article will entitle you for four (4) CPD Hours. As part of the incentive scheme of IEM, the following are applicable:

a) Referee more than three (3) papers vetted in a year
A token of appreciation e.g. IEM souvenirs
b) Referee more than five (5) papers vetted in a year
Invitation to IEM Annual Dinner alone
c) Referee ten (10) papers or more
Invitation to IEM Annual Dinner with spouse

On the other hand, failure to respond to three (3) articles will automatically deregister you from the vetters list.

Thank you for your support.

Note:
All correspondences are to be address to:
The Chief Editor
Standing Committee on Publications
The Institution of Engineers, Malaysia,
Bangunan Ingenieur, Lots 60&62, Jalan 52/4,
P.O.Box 223, (Jalan Sultan) 46720 Petaling Jaya, Selangor.
(Forms could be obtained at IEM)*